Influence of Magnesium Incorporation on the Structural, Optical, and Electronic Properties of Chemically Synthesized ZnO Thin Films: Experimental Observations and Ab Initio Analysis

Salah OUDJERTLI[1,a,*], Abdelkader MOHAMMEDI[2,b], Miloud IBRIR[2,c]
[1] Research Center in Industrial Technologies. (CRTI). BP 64, Roade of Dely Brahim, Cheraga 16014, Algiers, Algeria
[2] Laboratory of Materials Physics and its Applications, University of M'sila Department of Physics Algeria
Email: salah.oudjertli@gmail.com

ABSTRACT

In this study, zinc oxide (ZnO) thin films doped with varying amounts of magnesium (Mg) were fabricated through a sol–gel process combined with spin coating. The influence of Mg incorporation on the structural, electrical, and optical behaviors of ZnO layers was thoroughly examined. X-ray diffraction confirmed that all prepared coatings exhibit a wurtzite-type hexagonal lattice with strong preferential growth along the c-axis. Within the visible spectrum, the films demonstrated an average optical transmittance of approximately 77 %, while increasing Mg content induced a noticeable red shift in the absorption edge. Furthermore, the electronic characteristics of ZnO were investigated using UV–visible spectroscopy and optical microscopy. Complementary *ab initio* simulations determined a band gap of 3.2 eV, with calculated density of states in excellent agreement with the measured optical responses. These outcomes highlight the capability of *ab initio* methods to reliably describe the electronic properties of ZnO-based materials.

Keywords: Mg-doped ZnO, Thin Films, Spin Coating, UV–vis, Optical Microscope, FP-LAPW

1. INTRODUCTION

Zinc oxide (ZnO) belongs to the II–VI group of transparent semiconductor materials and naturally exhibits n-type conductivity at ambient conditions, accompanied by a high exciton binding energy. Due to these intrinsic properties, ZnO has attracted significant research interest for a wide range of technological uses, including optoelectronic devices, catalytic processes, and gas-sensing systems. Its abundance in the Earth's crust, combined with its non-toxic nature, also makes it a promising candidate for transparent conductive layers in thin-film photovoltaic cells.

In the present work, ZnO nanoparticles were examined through ultraviolet–visible spectroscopy (UV–vis), optical microscopy (OM), *and* first-principles computational approaches to assess their electronic behavior. Thin films composed of undoped ZnO and ZnO incorporating magnesium were produced via a sol–gel synthesis followed by spin coating at room temperature. The primary objective was to evaluate how Mg incorporation influences the structural and optical responses of ZnO thin films. Structural information was obtained through X-ray diffraction (XRD), while optical features were studied using UV–vis spectroscopy. The experimental outcomes were further discussed in relation to relevant findings reported in prior literature.

2. EXPERIMENTAL DETAIL

In this work, magnesium-doped zinc oxide (ZnO) thin films were synthesized with Mg concentrations ranging from 0 to 4 mol% using a sol–gel process followed by spin coating. Zinc acetate dihydrate and magnesium chloride hexahydrate served as the respective Zn and Mg precursors. Both compounds were dissolved in 2-propanol to obtain a final solution with a total concentration of C_T =0.49 M and a volume V_T = 9.9 mL. Monoethanolamine (MEA) was introduced as a chelating agent at a molar ratio of MEA/Zn = 1, ensuring the formation of transparent and homogeneous sols after continuous stirring at 60 °C for two hours on a temperature-controlled magnetic stirrer.

Prior to film deposition, glass substrates were cleaned by immersion in an ultrasonic bath containing a diluted sulfuric acid solution for ten minutes, then rinsed thoroughly with deionized water and dried under a stream of hot air. The coating procedure was carried out at a spin speed of 3000 rpm for 30 s, with the substrates preheated to 250 °C for four minutes

13th Annual International Conference on Material Science and Environmental Engineering (MSEE 2025), edited by Ke Wang, Helena Cristina Vasconcelos, Mohamed Mahmoud Gomaa, Proc. of SPIE Vol. 13811, 1381102 · © The Authors. Published under a Creative Commons Attribution CC-BY 4.0 License · doi: 10.1117/12.3087223

between successive layers to promote solvent evaporation. This sequence was repeated until the desired film thickness was achieved. The coated substrates were then annealed in air at 500 °C for 90 minutes, leading to the formation of high-quality Mg-doped ZnO films. This combined sol–gel/spin-coating strategy provided a reproducible route to obtaining uniform and well-adhered thin layers suitable for subsequent characterization.

2.1 CHARACTERIZATION METHOD

The surface morphology and crystal structure of the synthesized ZnO:Mg thin films (0–4 mol% Mg) were examined using X-ray diffraction (XRD). Measurements were carried out on a Rigaku Ultima IV diffractometer operating in the Bragg–Brentano geometry with Cu–Kα radiation (λ = 0.154 nm).
Optical characterization included the determination of transmittance (T) and absorbance (A) spectra at ambient temperature, recorded in the 300–800 nm wavelength range with a Perkin Elmer Lambda 35 UV–vis spectrophotometer. Additionally, the structural and morphological features of high-purity ZnO powder (99.9%) were analyzed using both ultraviolet–visible–infrared spectroscopy (UV–vis) and optical microscopy (OM). Observations of particle size distribution and surface texture were performed with a NIKON ECLIPSE LV150N optical microscope, enabling detailed imaging of the sample morphology.

2.2 COMPUTATIONAL DETAILS

Theoretical simulations were performed using the full-potential linearized augmented plane wave (FP-LAPW) approach, as implemented in the WIEN2k software package [1], within the framework of density functional theory (DFT) [2,3]. For the evaluation of structural parameters, the exchange–correlation interactions were treated using both the local density approximation (LDA) and the generalized gradient approximation (GGA) in their standard formulations. In order to refine the description of the electronic band structure, the Engel–Vosko scheme was applied, providing improved accuracy for energy-dependent properties.

3. RESULTS AND DISCUSSION

3.1. STRUCTURAL CHARACTERIZATION

Figure 1a. illustrates the X-ray diffraction (XRD) profiles obtained for Mg-doped ZnO thin films containing 0, 2, and 4 mol% magnesium. All observed diffraction maxima can be indexed to the hexagonal wurtzite structure of ZnO. The most intense reflection appears at the (002) plane, indicating a preferential orientation along the c-axis and suggesting vertical alignment of ZnO nanorods. This preferential growth is generally attributed to the lower surface energy of the (002) facet, making it the most thermodynamically stable orientation [4].
As displayed in Figure 1b and summarized in Table 1, both the peak intensity and the full width at half maximum (FWHM) of the (002) reflection decrease as Mg content increases. This trend is indicative of high crystallinity in the as-grown films, and the structural quality compares favorably with ZnO layers obtained through other deposition techniques such as spray pyrolysis or atomic layer deposition [5,6].
The lattice parameters a = b and c, the positional parameter u of the wurtzite structure, the Zn–O bond length L, and the crystallite size D were derived using the relationships given in Equations (1)–(4) [7–10]. These structural metrics provide quantitative insight into the influence of Mg incorporation on the ZnO crystal lattice.

$$\frac{1}{d_{hkl}^2} = \frac{4}{3}\left(\frac{h^2+hk+k^2}{a^2}\right) + \frac{l^2}{c^2} \tag{1}$$

$$u = \frac{a^2}{3c^2} + \frac{1}{4} \tag{2}$$

$$L = \sqrt{\left(\frac{a^2}{3} + \left(\frac{1}{2} - u\right)^2 c^2\right)} \tag{3}$$

$$D = \frac{0.9\lambda}{(\beta_{obsv}^2 - \beta_{inst}^2)^{\frac{1}{2}} cos\theta} \tag{4}$$

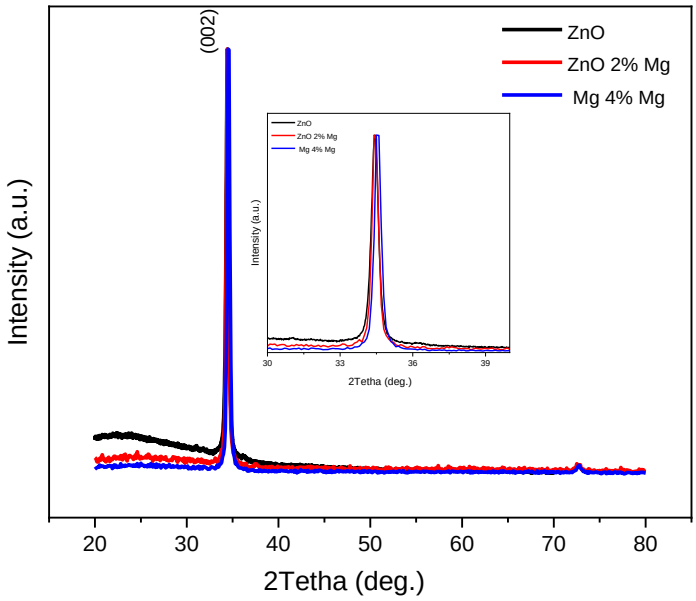

Fig. 1 *(a)* X-ray diffraction spectra of ZnO thin films doped with various magnesium concentrations, showing the characteristic wurtzite peaks. *(b)* Variation in the position of the (002) diffraction peak as a function of Mg content.

The X-ray wavelength (λ) used in the measurements was 0.154 nm, while θ represents the Bragg diffraction angle. The observed broadening of the diffraction peak is quantified by its full width at half maximum (FWHM), denoted β_{obsv} , whereas β_{inst} corresponds to the instrumental contribution, both expressed in radians.

As reported in Table 1, the undoped ZnO film exhibits its (002) diffraction maximum at 2θ = 34.475°. Increasing the Mg content results in a shift of this peak toward higher angles, which reflects a contraction of the lattice constants and a decrease in the Zn–O bond length L compared to the undoped material.

Table 1 compiles the key structural parameters, including the FWHM values, lattice constants a and c, bond length L, the wurtzite positional parameter u, and the crystallite size D, thus offering a complete overview of the structural evolution as a function of Mg doping.

Samples	2θ [deg.]	FWHM[deg.]	a [Å]	c [Å]	u	L [Å]	D [nm]
0% Mg	34.475	0.351	3.2772	5.2257	0.390	1.998	25.280
2% Mg	34.556	0.291	3.2564	5.2351	0.389	1.967	31.751
4% Mg	34.665	0.363	3.2663	5.1836	0.391	1.957	25.651

The results obtained in this work align closely with previous reports [11–15] concerning crystallite size evolution. When the magnesium content in the precursor solution was increased from 2% to 4%, the average crystallite size decreased from 31.5 nm to 25.8 nm. This reduction can be attributed to the defect generation within the ZnO crystal lattice caused by Mg incorporation, which hinders grain growth. Ghahramanifard et al. [13] associated this effect with Zener pinning, while Roguai et al. [14] linked it to the segregation of Mg atoms at grain boundaries.

Interestingly, at the highest Mg concentration studied (4%), the crystallite size increased to 35.6 nm, which is likely due to the substitution of Zn^{+2} ions by Mg^{+2} ions in the lattice [12]. Furthermore, progressive Mg addition was found to lower both the dislocation density and the lattice strain, suggesting an improvement in crystal quality as Mg ions replace Zn ions

at specific lattice sites [14]. Similar trends have been reported for Fe-doped ZnO [16] and V-doped ZnO films prepared by the sol–gel method [17].
In addition, the observation of negative stress values along the c-axis indicates the presence of compressive forces in the films. This effect is likely caused by mismatches in the thermal expansion coefficients between the ZnO layers and the glass substrates used during the deposition process [18].

3.2. OPTICAL CHARACTERIZATION

Figure 2 illustrates the variations in optical transmittance and reflection coefficients of the films over the wavelength range of 300–800 nm. For the undoped ZnO sample, the average transmittance in the visible spectrum reaches approximately 85%, with the absorption edge located near 380 nm. This behavior arises from the wide band gap of ZnO, which permits the passage of visible light while effectively blocking ultraviolet radiation.
Upon increasing the Mg concentration, minor changes are detected in both the transmittance within the visible range and the position of the absorption edge, as shown in Figure 2. The optical band gap energy (Eg) was determined using Tauc's method [19], applying the relationships expressed in Equations (5) and (6). These calculations provide insight into the electronic transitions and how Mg incorporation influences the optical properties of the ZnO matrix.

$$(\alpha h\nu)^n = B\left(h\nu - E_g\right) \tag{5}$$

Where B is a constant, n=2 for direct band gap energy, and α the absorption coefficient obtained by:

$$\alpha = \frac{1}{t} Ln\left(\frac{1}{T}\right) \tag{6}$$

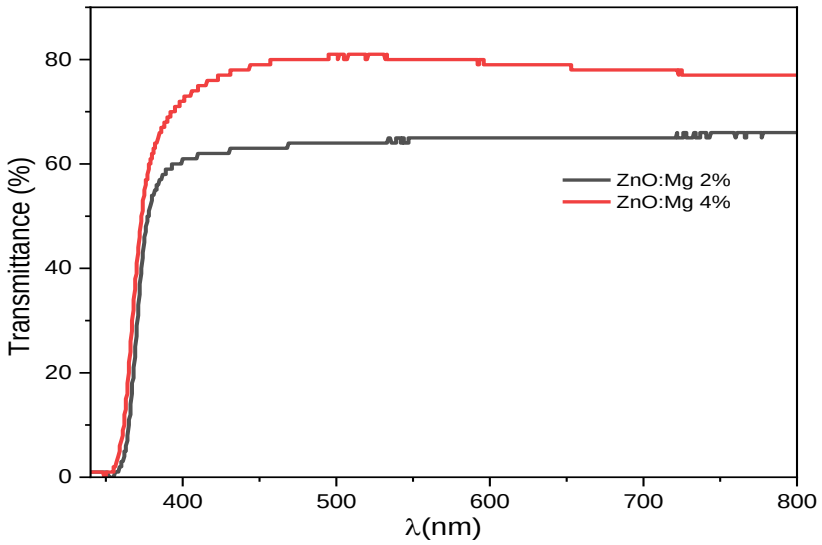

Fig. 2. Optical transmittance of Mg-doped ZnO films.

Ultraviolet–visible–infrared (UV–vis–IR) spectroscopy was employed to investigate the optical behavior of ZnO powders. UV–vis spectroscopy relies on the interaction between photons and matter, allowing for the measurement of both absorption and transmission spectra in the ultraviolet and visible regions—hence its designation.
Figure 3 displays the absorption spectrum obtained from the UV–vis analysis of the ZnO powder. This technique was applied to quantify the optical absorption characteristics of the sample. The spectrum exhibits a pronounced peak at approximately 375 nm, corresponding to an energy of 3.15 eV. Variations in particle size within the powder lead to slight shifts in the absorption maximum. For bulk ZnO, the typical band gap is around 3.37 eV; however, at the nanoscale, the band gap widens due to quantum confinement effects.

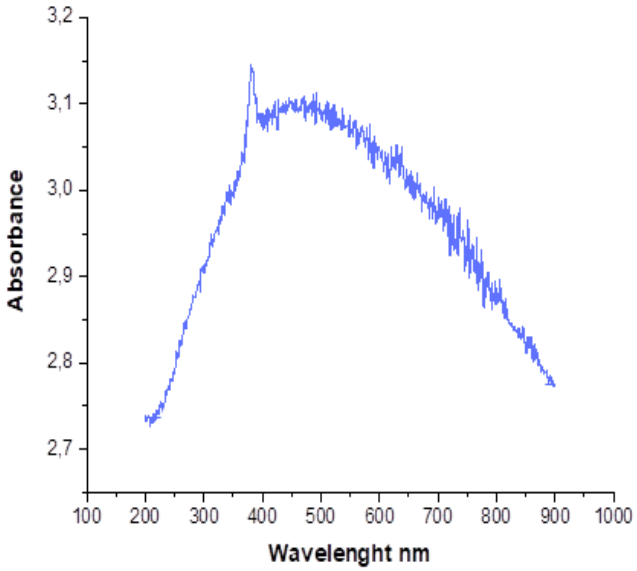

Fig. 3. UV–vis absorption spectrum of the ZnO powder.

3.3. PARTICLE MORPHOLOGY

ZnO powders were characterized by an optical microscope, NIKON ECLIPSE LV150N equipment. **Figure 4.** presents the micrographs obtained with an optical microscope, which reveal a colorful image with magnifications of 10x3 and 50x3 and a particle size of randomly scattered particles of varying sizes, ranging from a few micrometers to several tens, and a heterogeneous particle size distribution.

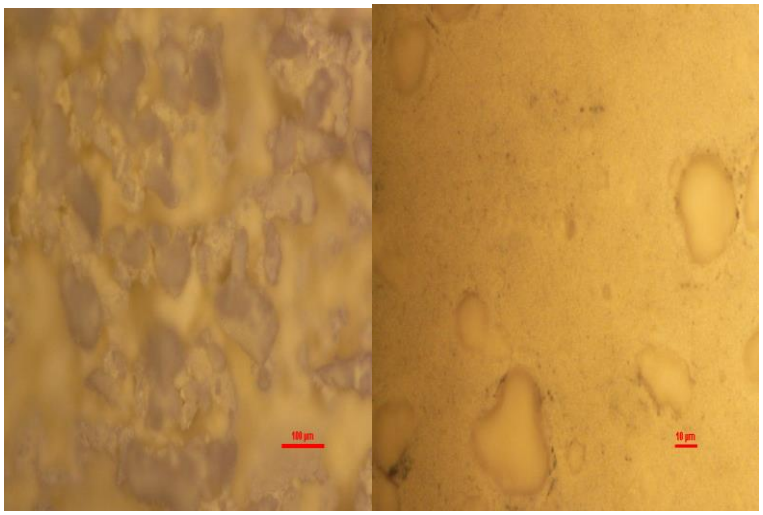

Fig. 4. Optical microscopy image of ZnO powder, showing particles of various sizes and irregular spatial distribution.

3.4. FIRST PRINCIPAL CALCULATIONS

In this work, first-principles calculations were carried out to explore the electronic properties of ZnO in its different structural configurations. The rocksalt phase of ZnO was examined by determining both the optimized lattice geometry and the self-consistent electronic band structure. Total energy computations were performed for several crystal configurations, with the unit-cell volume varied around its equilibrium value. The relationship between total energy and cell volume for the B1 phase of ZnO is presented in Figure 5.

The structural parameter "a" was found to be 4.28Å for rocksalt structures which can be described by it. Using GGA approximation, an obtained reasonable agreement with published data [20, 21] in terms of volume calculation was observed. Furthermore, using GGA approximation, both band structure and total energy states at equilibrium volumes were calculated in **Figure 6**. For phase B1, an equilibrium volume value of 19.54Å3 was computed using GGA approximation that aligns well with previously published results [22].

Zinc oxide is identified as an indirect bandgap semiconductor having a gap size equaling 0.81 eV in the case of the B1 phase. However experimental values show significantly larger pure zinc oxide gap sizes than those calculated from LDA or GGA codes; although Mao et al.(2008) reported slightly higher values around 1eV [23].

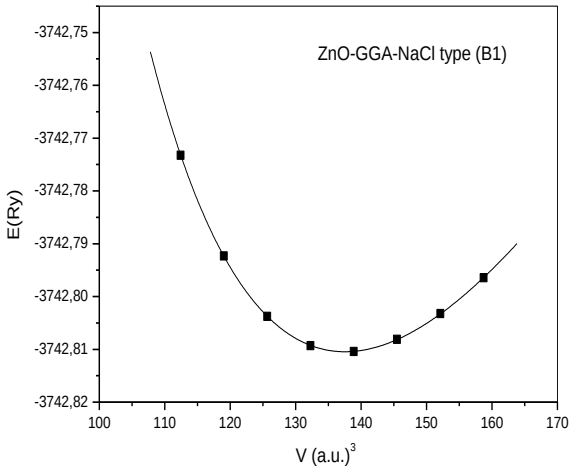

Fig.5 Total energy variation as a function of unit-cell volume for the B1 phase of ZnO, obtained from GGA calculations.

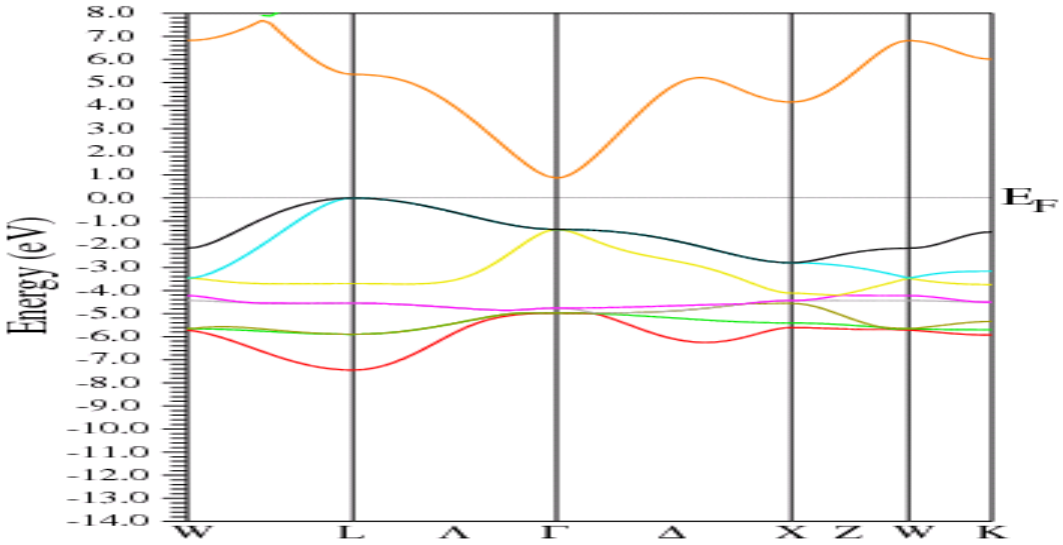

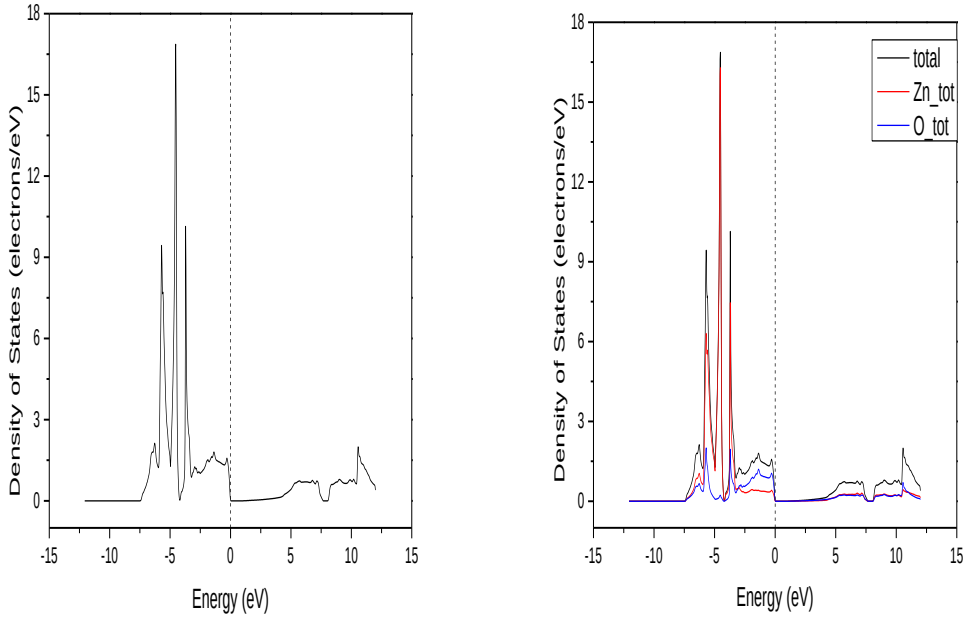

Fig. 6. Calculated density of states (DOS) for ZnO in the B1 phase, plotted as a function of energy (color version available online).

4. CONCLUSION

Thin films of Mg-doped ZnO containing 0%, 2%, and 4% Mg were deposited onto glass substrates via a sol–gel synthesis combined with spin coating. The purpose of the study was to assess how progressive magnesium incorporation influences the morphology, structural parameters, and both linear and nonlinear optical behaviors of the films. Increasing Mg concentration induced noticeable distortions in certain crystallographic parameters, along with variations in the aaa and ccc lattice constants. The average crystallite size increased from 25.45 nm to 35.53 nm, while the dislocation density and lattice strain decreased, indicating improved crystalline quality.

Optical characterization revealed modifications to the band gap as Mg content increased. The refractive index dispersion was well described by a single-oscillator model, and the associated parameters E0, Ed, and n∞ _\inftyn∞ were determined experimentally. Overall, the magnesium-doped ZnO layers prepared in this work displayed superior optoelectronic characteristics compared with values reported in earlier studies, and they exhibited a stronger nonlinear optical response than their undoped ZnO counterparts.

Moreover, ultraviolet–visible–infrared (UV–vis–IR) spectroscopy, along with ZnO sputtering techniques, was employed to assess various absorption characteristics. Optical microscopy provided visualizations of ZnO replicas, revealing particles irregularly dispersed across the sample, with dimensions ranging from a few micrometers to several tens of micrometers.

Complementary first-principles simulations indicated that the electronic features identified were specific to the rocksalt phase, with no correspondence to those of pure wurtzite ZnO. The experimental data obtained in this work showed strong agreement with previously reported theoretical predictions, which classify zinc oxide in the B1 phase as an indirect band gap semiconductor.

REFERENCES

[1] P. Blaha, K. Schwarz, G.K. Madsen, D. Kvasnicka, J. Luitz, wien2k, An augmented plane wave+ local orbitals program for calculating crystal properties, 60 (2001).

[2] P. Hohenberg, W. Kohn, Inhomogeneous electron gas, Physical review, 136 (1964) B864.

[3] W. Kohn, L.J. Sham, Self-consistent equations including exchange and correlation effects, Physical review, 140 (1965) A1133.
[4] A. Mhamdi, A. Boukhachem, M. Madani, H. Lachheb, K. Boubaker, A. Amlouk, M. Amlouk, Study of vanadium doping effects on structural, opto-thermal and optical properties of sprayed ZnO semiconductor layers, Optik-International Journal for Light and Electron Optics, 124 (2013) 3764-3770.
[5] K. Tapily, D. Gu, H. Baumgart, Growth mechanism of ALD ZnO films investigated by physical characterization, ECS Transactions, 33 (2010) 355.
[6] E. Andrade, M. Miki-Yoshida, Growth, structure and optical characterization of high quality ZnO thin films obtained by spray pyrolysis, Thin solid films, 350 (1999) 192-202.
[7] O. Lupan, T. Pauporté, L. Chow, B. Viana, F. Pellé, L.K. Ono, B.R. Cuenya, H. Heinrich, Effects of annealing on properties of ZnO thin films prepared by electrochemical deposition in chloride medium, Applied Surface Science, 256 (2010) 1895-1907.
[8] G. Srinivasan, R. Rajendra Kumar, J. Kumar, Li doped and undoped ZnO nanocrystalline thin films: a comparative study of structural and optical properties, Journal of sol-gel science and technology, 43 (2007) 171-177.
[9] R. Mariappan, V. Ponnuswamy, A.C. Bose, A. Chithambararaj, R. Suresh, M. Ragavendar, Structural, optical and electrical characterization of nebulizer-sprayed ZnO nano-rods, Superlattices and Microstructures, 65 (2014) 184-194.
[10] J. Sengupta, A. Ahmed, R. Labar, Structural and optical properties of post annealed Mg doped ZnO thin films deposited by the sol–gel method, Materials Letters, 109 (2013) 265-268.
[11] M.H. Forouzanfar, P. Liu, G.A. Roth, M. Ng, S. Biryukov, L. Marczak, L. Alexander, K. Estep, K.H. Abate, T.F. Akinyemiju, Global burden of hypertension and systolic blood pressure of at least 110 to 115 mm Hg, 1990-2015, Jama, 317 (2017) 165-182.
[12] S. Muthukumaran, R. Gopalakrishnan, Structural, FTIR and photoluminescence studies of Cu doped ZnO Properties of High-Quality ZnO Thin Films Obtained by Spin-Coating Technique, physica status solidi (b), 258 (2021) 2000472.nanopowders by co-precipitation method, Optical Materials, 34 (2012) 1946-1953.
[13] F. Ghahramanifard, A. Rouhollahi, O. Fazlolahzadeh, Electrodeposition of Cu-doped p-type ZnO nanorods; effect of Cu doping on structural, optical and photoelectrocatalytic property of ZnO nanostructure, Superlattices and Microstructures, 114 (2018) 1-14.
[14] S. Roguai, A. Djelloul, A structural and optical properties of Cu-doped ZnO films prepared by spray pyrolysis, Applied Physics A, 126 (2020) 122.
[15] A. Mohammedi, M. Ibrir, O. Meglali, S. Berri, Influence of Cu-Doping on Linear and Nonlinear Optical
[16] S. Ilican, Y. Özdemir, M. Caglar, Y. Caglar, Temperature dependence of the optical band gap of sol-gel derived Fe-doped ZnO films, Optik, 127 (2016) 8554-8561.
[17] Q. Fan, D. Li, J. Li, C. Wang, Structure and piezoelectricity properties of V-doped ZnO thin films fabricated by sol-gel method, Journal of Alloys and Compounds, 829 (2020) 154483.
[18] A. Moreh, B. Hamza, S. Abdullahi, A. Bala, Z. Abdullahi, M. Shehu, Effect of Post Annealing Temperature on Structural Properties of ZnS thin films Grown by Spray Pyrolisis Technique, International Journal of Innovation and Applied Studies, 9 (2014) 913-917.
[19] A. Kaphle, P. Hari, Enhancement in power conversion efficiency of silicon solar cells with cobalt doped ZnO nanoparticle thin film layers, Thin Solid Films, 657 (2018) 76-87.
[20] H. Karzel, W. Potzel, M. Köfferlein, W. Schiessl, M. Steiner, U. Hiller, G. Kalvius, D. Mitchell, T. Das, P. Blaha, Lattice dynamics and hyperfine interactions in ZnO and ZnSe at high external pressures, Physical Review B, 53 (1996) 11425.
[21] S. Desgreniers, High-density phases of ZnO: Structural and compressive parameters, Physical Review B, 58 (1998) 14102.
[22] A.H. Reshak, Z. Charifi, H. Baaziz, First-principles study of the optical properties of PbFX (X= Cl, Br, I) compounds in its matlockite-type structure, The European Physical Journal B, 60 (2007) 463-468.
[23] Y. Mao, J. Zhong, Y. Chen, First principles study of the band structure and dielectric function of (6, 6) single-walled zinc oxide nanotube, Physica E: Low-dimensional Systems and Nanostructures, 40 (2008) 499-502.